



Published in final edited form as:

Hum Mutat. 2014 November ; 35(11): 1342–1353. doi:10.1002/humu.22680.

Comprehensive Analysis of Pathogenic Deletion Variants in Fanconi Anemia Genes

Elizabeth K. Flynn¹, Aparna Kamat¹, Francis P. Lach², Frank X. Donovan³, Danielle C. Kimble¹, Narisu Narisu³, Erica Sanborn², Farid Boulad⁴, Stella M. Davies⁵, Alfred P. Gillio III⁶, Richard E. Harris⁵, Margaret L. MacMillan⁷, John E. Wagner Jr.⁷, Agata Smogorzewska², Arleen D. Auerbach^{8,*}, Elaine A. Ostrander¹, and Settara C. Chandrasekharappa^{1,*}

¹Cancer Genetics Branch, National Human Genome Research Institute, NIH, Bethesda, MD 20892

²Laboratory of Genome Maintenance, The Rockefeller University, New York, NY 10065

³Genome Technology Branch, National Human Genome Research Institute, NIH, Bethesda, MD

⁴Memorial Sloan Kettering Cancer Center, 1275 York Avenue, New York, NY 10065

⁵Cincinnati Children's Hospital Medical Center, Cincinnati, OH 45229

⁶Hackensack UMC, Hackensack, NJ 07601

⁷University of Minnesota, Delaware St. SE, Minneapolis, MN 55455

⁸Human Genetics and Hematology Program, The Rockefeller University, New York, NY 10065

Abstract

Fanconi anemia (FA) is a rare recessive disease resulting from mutations in one of at least 16 different genes. Mutation types and phenotypic manifestations of FA are highly heterogeneous and influence the clinical management of the disease. We analyzed 202 FA families for large deletions, using high-resolution Comparative Genome Hybridization arrays (arrayCGH), Single Nucleotide Polymorphism arrays (SNParrays) and DNA sequencing. We found pathogenic deletions in 88 *FANCA*, seven *FANCC*, two *FANCD2*, and one *FANCB* families. We find 35% of FA families carry large deletions, accounting for 18% of all FA pathogenic variants. Cloning and sequencing across the deletion breakpoints revealed that 52 *FANCA* deletion ends, and one *FANCC* deletion end extended beyond the gene boundaries, potentially affecting neighboring genes with phenotypic consequences. Seventy-five percent of the *FANCA* deletions are *Alu-Alu* mediated, predominantly by *AluY* elements, and appear to be caused by Non-Allelic Homologous Recombination. Individual *Alu* hotspots were identified. Defining the haplotypes of four *FANCA* deletions shared by multiple families revealed that three share a common ancestry. Knowing the

*Correspondence to: Settara C. Chandrasekharappa, Cancer Genetics Branch, National Human Genome Research Institute, National Institutes of Health, 50 South Drive, Building 50, Room 5232, Bethesda MD. chandra@mail.nih.gov or Arleen D. Auerbach, Human Genetics and Hematology Program, The Rockefeller University, 1230 York Avenue, New York, NY. auerbac@mail.rockefeller.edu.

Disclosure Statement: The authors declare no conflict of interest.

exact molecular changes that lead to the disease may be critical for a better understanding of the FA phenotype, and to gain insight into the mechanisms driving these pathogenic deletion variants.

Keywords

Fanconi anemia; array CGH; *FANCA*; *FANCB*; *FANCC*; *FANCD2*

INTRODUCTION

Fanconi anemia (FA) is a rare autosomal or X-linked recessive disorder, characterized by congenital malformations, bone marrow failure, and predisposition to cancer, particularly hematological malignancies and solid tumors of the head and neck. The classic characteristic of FA cells is the increased sensitivity to DNA-interstrand cross-linking agents such as diepoxybutane (DEB) (Auerbach, 2009). FA is genetically heterogeneous, resulting from mutations in one of the 16 known FA genes (FA Mutation Database, <http://www.rockefeller.edu/fanconi/>), including *FANCA* (MIM# 607139), *FANCB* (MIM# 300515), *FANCC* (MIM# 613899), *FANCD1* (MIM# 605724)/*BRCA2* (MIM# 600185), *FANCD2* (MIM# 613984), *FANCE* (MIM# 613976), *FANCF* (MIM# 613897), *FANCG* (MIM# 602956), *FANCI* (MIM# 611360), *FANCI* (MIM# 609054)/*BRIP1* (MIM# 605882), *FANCL* (MIM# 608111), *FANCM* (MIM# 609644), *FANCN* (MIM# 610832)/*PALB2* (MIM# 610355), *FANCO* (MIM# 613390)/*RAD51C* (MIM# 179617), *FANCP* (MIM# 613951)/*SLX4* (MIM# 613278), *FANCO* (MIM# 615272)/*ERCC4* (MIM# 133520) (Bogliolo, et al., 2013; Neveling, et al., 2009). The proteins encoded by these genes participate in pathways that are involved in detection and resolution of DNA-interstrand crosslinks, maintenance of hematopoietic stem cells, and prevention of tumorigenesis (Kottemann and Smogorzewska, 2013).

FANCA, *FANCC* and *FANCG* pathogenic variants account for the disease in 60%, 15%, and 10% of FA families, respectively, while mutations in the other genes occur less frequently (0.1%–4%) (Neveling, et al., 2009). The mutation spectrum includes single nucleotide variations (SNV), small insertions and deletions (INDELs), and large deletions. Large deletions contribute 20–40% of all *FANCA* mutations (Castella, et al., 2011; Centra, et al., 1998; Levrán, et al., 1998; Moghrabi, et al., 2009; Morgan, et al., 1999). The majority of these deletions were identified by Multiplex Ligation Probe Analysis (MLPA), identifying deleted exons only, but not the precise breakpoints.

Although the majority of pathogenic variants associated with FA are private germline variants, a few common founder mutations have been reported (Amouri, et al., 2014; Auerbach, et al., 2003; Callen, et al., 2005; Castella, et al., 2011; de Vries, et al., 2012; Morgan, et al., 2005; Tipping, et al., 2001; Whitney, et al., 1993). Most of the founder mutations were identified after extensive sequencing efforts and haplotype analysis of populations with a high prevalence of disease, and are primarily SNV and INDELs. The identification of founder pathogenic variants has facilitated the screening for carriers of these variants among unaffected individuals within these select populations. To identify and confirm if a large deletion could be a founder mutation requires precise determination of the

deletion breakpoints at the single nucleotide level, which is not possible using the MLPA method.

Knowing the exact molecular changes that lead to disease may be critical for clinical management of the patient, especially for reproductive counseling. We have initiated application of high throughput, state of the art methodologies to identify all disease-causing variants in ~300 FA families enrolled in the International Fanconi Anemia Registry (IFAR). As a part of this effort, we initially screened 202 FA families for deletions, using comparative genomic hybridization arrays (aCGH) and single nucleotide polymorphism (SNP) arrays. We designed custom CGH arrays for simultaneous screening of deletions in 15 FA and other functionally relevant genes (the 16th FA gene, *FANCO*, was recently identified and is thus not included in our array design). The arrays were designed to cover the entire length of each gene plus up to 200kb on either side, enabling us to determine the precise boundaries of deletions extending beyond an FA gene locus. We identified deletions in 98 FA families in four different FA genes, of which 90% were in the *FANCA* gene. The high resolution analysis of the deletion boundaries identified by aCGH, accompanied by subsequent cloning and sequencing of the breakpoints, provides insight into the location and potential mechanisms driving the intrachromosomal breakage events, in addition to identifying conserved deletions and their likely origin.

MATERIALS AND METHODS

Study Subjects

Genomic DNA samples were from individuals diagnosed with FA and registered in the International Fanconi Anemia Registry (IFAR), following written informed consent. These studies were approved by the Institutional Review Board of the Rockefeller University, New York, USA. The Office of Human Subjects Research at the National Institutes of Health and Institutional Review Board of the National Human Genome Research Institute (NHGRI) approved the reception of de-identified cell lines and DNA samples from The Rockefeller University and analysis of the underlying molecular variants. Genomic DNA was isolated from peripheral blood, fibroblasts, or EBV immortalized cell lines. The Puregene kit and the DNeasy blood & tissue DNA extraction kit (Qiagen, Inc) were used for DNA extraction from blood and cell lines respectively. Phenol/chloroform extraction and ethanol precipitation was included as a final step in the preparation of DNA.

arrayCGH

A custom CGH 12×135K Array was designed using NimbleDesign (NimbleGen, Madison, WI). It consisted of 134,490 50mer probes (44,830 probes in triplicates) selected with an interval of 37 base pairs (bp). Unique probes were selected. The design covered the entire length and up to 200 kb on both sides of all the FA genes (except the recently identified *FANCO*) and twelve other functionally relevant genes (Supp. Table S1). DNA from patients and reference DNA (human male DNA from Promega, Madison, WI) were labeled with different fluorochromes, mixed, and hybridized to the 12×135,000 array. We used NimbleGen Service for CGH and thus the manufacturing, hybridization, scanning, and preliminary analysis was performed at their processing facility in Iceland. The data analysis

was performed using NimbleScan and the intensity variations were visualized and displayed using SignalMap; both softwares were developed by NimbleGen. The genomic coordinates are based on the human genome build hg18 (NCBI36.1).

SNP array

Genotyping was performed using the HumanCytoSNP, HumanOmniExpress or HumanOmni2.5Quad DNA analysis BeadChip kit (Illumina, Inc.), representing 300,000, 750,000 and 2.5 million SNPs respectively. Genomic DNA (300ng) was processed per the Illumina “infinium assay” protocol (Gunderson, et al., 2005). In brief, this included whole-genome amplification and fragmentation of DNA, hybridization to the BeadChip with specific oligonucleotide probe array (50-mers), enzymatic extension of the 3' terminal base for incorporation of the allele specific nucleotide, detection with fluorescently tagged reagent and signal amplification. The allele type and its intensity were collected using BeadArray scanner, and visualized with the GenomeStudio (v2009.2, www.Illumina.com) genotyping module. The deletion intervals in two families with larger deletions were determined using the intensity data using the same program.

PCR, Cloning and Sequencing of Breakpoints

Multiple primer sets were designed 500bp to 2000bp flanking the breakpoint ends as determined by aCGH or SNP array. Amplification reactions were carried out with 10–15 nanograms (ng) of genomic DNA using KOD Extreme (EMDmillipore) enzyme according to the manufacturer recommendations with the addition of GC melt (Clontech). Initial 15 cycles of PCR, each with 0.5°C decreasing annealing temperature per cycle starting at 65°C was followed by 25 cycles at 57°C annealing temperature. Amplification products were analyzed by agarose gel electrophoresis, and the chosen products were purified from gel using Qiaquick gel extraction kit (Qiagen). Purified products were A-tailed with Taq polymerase and cloned using TOPO TA-cloning kit (Life Technologies). Clones were screened by colony PCR, plasmid DNA was purified from positive clones using Qiaprep spin miniprep kit (Qiagen), and subjected to cycle sequencing using BigDye v3.1 (Applied Biosystems). Sequences were aligned to the human reference genome build hg18 (NCBI36.1) using the BLAT program (www.genome.ucsc.edu).

Haplotype Analysis

Genotypes of the proband and their parental DNA were collected using high-density SNP arrays as described above. Haplotypes associated with the *FANCA* conserved deletions, CD2 and CD4–6, and the *FANCC* conserved deletion were determined using SNP genotypes from parental and proband DNA and analyzing the trios data with the -P1 function of PHASE v2.1 program (<http://www.stat.washington.edu/Stephens/software.html>) (Stephens and Donnelly, 2003; Stephens, et al., 2001). The output from this analysis along with knowledge of inheritance of each deletion allowed for the identification of the deleted allele. For *FANCA*, SNPs were chosen from chr16.hg18:g.88,235,597_88,513,344, and for *FANCC*, chr9.hg18:g.96,874,394_97,142,804. Only the SNPs that were also present in the HapMap Phased haplotype data (CEU, NCBI_Build36 rel22, <http://www.Hapmap.org>) were considered for analysis.

Phylogenetic Analysis

MEGA 5.1 (www.megasoftware.net) was used to perform a phylogenetic analysis on the *FANCA* common deletions. Phased haplotypes from the HapMap CEU population (Phase 2) were downloaded for use in the analysis as described above. We identified 51 unique CEU haplotypes for this genomic region as defined above. Of the 51 unique CEU haplotypes, four were excluded because each matched one of the seven haplotypes of the *FANCA* common deletions. The analysis consisted of 55 sequences: 47 unique haplotypes from the HapMap CEU population, seven haplotypes from the common deletions, and one from Chimp genome. The phylogeny reconstruction was performed using a Maximum Likelihood statistical method with 500 bootstrap replications. A Tamura-Nei substitution model was implemented with the assumption that the rates were uniform for all sites (as opposed to gamma distributed). Missing data was not evaluated and is indicated with a question mark.

RESULTS

ArrayCGH Analysis Reveals Deletions in *FANCA*, *FANCB*, *FANCC* and *FANCD2*

Genomic DNA from 202 FA families enrolled in the IFAR were screened for deletion variants by aCGH. The families chosen for analysis include 105 families with no prior screening for mutations, and 97 families for which one (69 families) or both mutations (28 families) were previously identified by various molecular methods including sequencing for SNV and INDELs and MLPA for larger deletions. Of the latter 97 families, 50 families (27 families with one mutation known and 23 families with both mutations known) were believed to carry deletions as determined by MLPA; however, precise breakpoint coordinates were lacking. Five families, for which both mutations were known from prior sequencing efforts, were used as negative controls for the array studies.

Genomic DNA samples from probands were screened for deletions for the entire length and up to 200kb on either side of 15 FA genes, plus twelve additional functionally relevant genes (Supp. Table S1) using aCGH. Deletion variants were found in 88 *FANCA*, one *FANCB*, seven *FANCC* and two *FANCD2* families (Table 1A, Supp. Figure S1). Two deletions, one *FANCA* and the *FANCB*, extended beyond the boundaries of the array design, and thus their deletion intervals were determined using genome-wide SNP arrays. For 48 of the 50 families previously thought to carry a deletion variant, as determined by other methods, the deletions were confirmed and breakpoints defined; however, two single-exon deletions originally observed by MLPA were not confirmed by CGH, and subsequent sequence analysis revealed that sequence variants in these exons reduced hybridization of MLPA probes, thus giving an erroneous result in the initial MLPA assay. Of the 105 FA families for which there was no prior knowledge of the FA gene or the pathogenic variants, deletions accounted for one of the germline variants in 34 families (32 in *FANCA* and two in *FANCD2*) and both pathogenic variants in two families (both in *FANCA*, one homozygous family and one compound heterozygous family) (Table 1B). Thirty-six of these 105 FA families carried a total of 38 deletions indicating nearly a third of FA families carry deletions, and that the deletions constitute ~18% of the total FA mutations (Table 1B).

Characterization of *FANCA* Deletions in 88 FA Families

While 78 families with deletions in *FANCA* were heterozygous for the deletion, ten families carried two deletions each; five probands carried distinct homozygous deletions, FAM12, FAM24, FAM26, FAM74, and FAM81 and the other five were compound heterozygotes resulting from two different deletions, FAM23, FAM28, FAM46, FAM47, and FAM63 (Table 1 and Figure 1). The two deletions in the compound heterozygote families overlapped with each other with the exception of FAM23, and parental DNA was screened to confirm the ends of the overlapping deletions when necessary. In total, 93 distinct *FANCA* deleted alleles were identified, counting the deletions in homozygous families as one allele. The extent of the *FANCA* deletions is shown in Figure 1. The deletions' sizes span a wide range from ~1kb to 545kb, with over half of the deletions falling between 5–30kb in length. The telomeric boundary of the largest deletion (FAM9) extended outside the design limits of the CGH array, and analysis using SNP array determined the deletion extended to the telomeric end of chr16. The deletions encompass as little as one exon within *FANCA* (FAM24, FAM30, FAM87, FAM42) or as large as the entire *FANCA* gene along with 18 additional neighboring genes FAM1 (Figure 1, Table 2, and Table 3). Deletion data were deposited in the FA Mutation Database (<http://www.rockefeller.edu/fanconi/>).

Fifty-two deletion ends were found to originate or terminate outside the boundaries of the *FANCA* gene, including twenty deletions starting centromeric to *FANCA* and 32 deletions ending telomeric to *FANCA* (Figure 1). Eight of these deletions have both ends extending beyond the *FANCA* gene. In total, 47% of the deletions extend beyond the limits of the *FANCA* gene and the majority of these also affect other neighboring genes (Supp. Table S2). Similarly, analysis of the *FANCA* deletions from the subset of 105 FA families (Table 1B) for which no mutations were known prior to this study revealed 19 of the 35 *FANCA* deletions or 54% extend beyond *FANCA*.

Cloning, Sequencing and Analysis of 68 *FANCA* Deletion Breakpoints

To further characterize the deletion breakpoints to the exact nucleotide, the region across the breakpoint junctions was amplified by designing multiple primer sets to a 500bp–2000bp region flanking the deletions. The resulting amplification products were purified, cloned, and sequenced. The primers used for cloning and sequencing of the breakpoints are listed in Supp. Table S3. Alignment of the sequences to the reference human genome identified the exact nucleotide positions of the breakpoints for 68 *FANCA* deletions. The results are summarized in Table 3 and the alignments are shown in Supp. Figure S2.

The extent of homology and the intervening sequences near the breakpoints reveal the likely mechanism(s) that cause the deletions, which are presented in Table 3 and Supp. Table S4 and summarized in Table 4. We find majority (50/68) of the deletions have both breakpoints occurring at *Alu* elements in the same orientation with significant homology and overlapping sequence ranging from four to 45bp. These appear to be driven by *Alu-Alu* mediated nonallelic homologous recombination (NAHR) (Gu, et al., 2008). Two deletions occur at *Alu* elements in opposite orientation, one shared in FAM46_d2, FAM63_d2, and FAM58–60 and the other in FAM18. The former lacks any overlapping sequence but instead has a 2bp insertion at the breakpoints, and thus appears to be mediated by nonhomologous end

joining (NHEJ), whereas the latter has overlapping sequence of 2bp and may be mediated by alternative end joining (alt-EJ). Nine of the twelve remaining breakpoints lack any significant homology surrounding the breakpoint junctions; FAMs 52 and 71 show 0–1 bp overlap and are anticipated to be driven by NHEJ, whereas the deletions in the other seven (FAMs 4, 10–11, 14, 18–19 and 32) with 2–4bp homology appear to be caused by alt-EJ (Gu, et al., 2008; Kidd, et al., 2010; Verdin, et al., 2013). The alignment of breakpoint sequences to the reference genome of the final three deletions, FAMs 30, 31, and 35, indicate a complex rearrangement potentially involving more than two genomic regions. All three deletions contain inserted sequences of 37bp, 29bp, and 179bp respectively, between the fully aligned breakpoint junctions (Supp. Figure S2, Supp. Table S4). The 37bp insertion in FAM30 aligns 100% in the antisense orientation at chr16.hg18:g.88350637_88350672, which is located within the deleted interval. The 29bp insertion in FAM31 could not be aligned to the genome reference sequence, and its origin is unclear. The 179bp insertion in FAM35 is of *AluY* origin. This *Alu* element is not present in reference genome at the breakpoint coordinates but BLAT aligns with high homology (99%) approximately 2 kb downstream from the telomeric breakpoint at chr16.hg18:g.88,373,127. Due to unavailability of parental DNA, we were unable to confirm whether this is a *de novo* insertion of an *Alu* element or an inherited event. Breakpoint junctions with insertions of >10bp, as observed in FAMs 30, 31, and 35, are thought to be caused by a replication-based mechanism termed FoSTeS/MMBIR (fork stalling and template switching/microhomology-mediated break induced repair) (Lee, et al., 2007).

Conserved Deletions (CD) in *FANCA* and their Haplotype Analysis

ArrayCGH indicated six deletions conserved in two or more seemingly unrelated families and sequence analysis confirmed these observations (Table 3, Figure 2B, Supp. Table S5). CD2 (FAM44 and FAM45), CD1 (FAM36–38), and CD5 (FAM75–79) shared among two, three and five families appeared to be caused by *Alu-Alu* mediated NAHR. CD6 was similar in three families, FAM81–83: sequencing however confirmed it was identical in FAM81 and FAM82 but the deletion in FAM83 shared the same *AluY* element at the centromeric breakpoint with FAM81 and FAM82 but targets an alternate *AluSc* element at its telomeric breakpoint. NAHR is the likely origin of CD6 deletions as well. However, CD3 (FAM50 and FAM51) with 2bp homology and CD4 (FAM46_d2, FAM63_d2, and FAM58–60) with 2bp insertion, appear to be caused by alt-EJ and NHEJ respectively.

We performed SNP analysis on the proband and parental DNAs to identify the haplotype for the allele with the deletion (referred to as the deleted allele) for families with CD2, CD4, CD5 and CD6. Due to lack of parental DNA, we were unable to collect SNP data and thus generate haplotypes for the families with CD1 and CD3. Using the PHASE program we were able to confidently establish the haplotype for the deleted alleles in families with CD2, CD4, CD5, and CD6. The results are summarized in Figure 2. For CD4 all five families were found to carry an identical haplotype on their respective deleted allele and support the hypothesis that this conserved mutation is probably the result of an ancient event. CD2 and CD5 each were identified on two very similar haplotypes, differing by just one SNP, and are also likely to be an ancient event. For CD2 and CD5, one of the haplotypes from each was found in the HapMap phased haplotypes and the other was not. CD6 was found in two

families on two very different haplotypes. This deletion therefore likely occurred independently in these two families (FAM81 and FAM82) thereby highlighting the breakpoints as potential hot spots. In support of this, the families are from different ethnic backgrounds, Caucasian and Hispanic (Supp. Table S5). In addition, FAM83 contains a very similar deletion interval as CD6, differing by just a few base pairs in the same *Alu* element at the centromeric end and a few hundred base pairs in an adjacent *Alu* element at the telomeric end of the deletion (Table 3). The similar deletions in FAM81 and FAM83 occur on the same haplotype and this haplotype is also found in the HapMap phased haplotype database.

FANCA Deletion Breakpoints Reside Predominantly in *AluY* SINE Elements

Distribution of the types of *Alu* at the *FANCA* locus and for 150kb of the extended region encompassing the *FANCA* gene, and the extent of breakpoints in each *Alu* type is shown in Figure 3. *AluSx* and *AluY* are equally represented as the highest percentage of SINE sequence, and the equal distribution of *AluSx* and *AluY* is not limited solely to the *FANCA* gene but to the extended 150 kb region as well. However, *AluY* elements have 40% more breakpoints than *AluSx* elements (Figure 3).

Locations of the deletion breakpoints and SINE elements within and around the *FANCA* gene are displayed in Figure 4. Despite the high number of available *Alu* elements in this region, some elements are targeted in multiple unique deletion events. Considering each conserved deletion as one deletion event which was caused by an ancient allele, with the exception of CD6, which may have occurred twice, there are 20 *Alu* elements involved in two or more deletions (Figure 4, Supp. Table S6).

Deletions in *FANCB*, *FANCC* and *FANCD2* Families

Three distinct deletions were identified in *FANCC* (Supp. Figure S1A, Table 2, and Table 3). Five families, FAM90–FAM94, share the deletion eliminating exon 3. Sequence analysis confirmed the shared deletion and an 18bp insertion at the breakpoint junction suggesting the deletion is likely caused by a fork stalling and template switching/microhomology-mediated break-induced replication (FoSTeS/MMBIR) mechanism (Table 3, Supp. Figure S2). Haplotype analysis could be performed for three of the five families carrying the conserved deletion (Figure 2D), and the three families shared the same haplotype, which supports the idea that deleted alleles are likely the result of a common ancestral mutation. The other two deletions, one encompassing exon one and regions upstream of the gene and one encompassing exon 8, were each found in one family, FAM95 and FAM89 respectively. The deletion breakpoints in FAM95 mapped precisely to the reference genome and had a “C” residue inserted at the breakpoint junction, suggesting NHEJ causing the deletion.

The heterozygous deletions in two *FANCD2* families were intragenic eliminating exon 18 (FAM98) or exons 2–17 (FAM97), whereas the hemizygous deletion in the *FANCB* family (FAM96) removed the entire gene and was large, requiring use of SNP array to determine the deletion boundaries (Table 2, Supp. Figure S1 B–C).

DISCUSSION

Knowing the molecular changes that lead to a disease is necessary for the advancement of “personalized” genomics and precision medicine (Couch, et al., 2014). The techniques we describe here can be employed toward precise molecular diagnosis of Fanconi anemia, which offers an increased potential for establishing genotype-phenotype relationships and translating these relationships to aid in management of the disease. The current study of deletions is part of our comprehensive effort to identify all the pathogenic variants for FA families in the IFAR. Recognizing that deletions contribute substantially to the mutation spectrum in *FANCA*, and that *FANCA* is mutated in 60% of FA patients, *FANCA* deletion analysis by MLPA was proposed as an initial step in a comprehensive mutation screening strategy earlier (Ameziane, et al., 2008). However, MLPA has primarily been limited to the identification of deleted *FANCA* exons and thus there has been very little effort to expand the screening for all FA genes at once and to define the precise molecular nature of the deletions.

Nearly a Third of FA Patients Carry Deletions, and Half of the *FANCA* Deletions Extend Beyond the Gene

Our study included screening for deletions in a subset of 105 families for which there was no prior data on the affected gene or the mutations causing the disease, and thus provided an evaluation of the extent of deletions in FA. We observed a third of these families carried deletions in FA genes. Though predominantly in *FANCA*, deletions were also observed in other FA genes, indicating that screening for deletions in all FA genes as described here is an invaluable tool in the molecular diagnosis of FA patients. The CGH array, though designed for high-resolution scan, may not reveal very small deletions; however, the lower limit is not clear. Our array design that allowed for scanning for deletions up to 200kb beyond the boundaries of FA genes, and precise mapping of the deletions allowed us to determine that half of the *FANCA* deletions extended beyond the boundaries of the gene. Thus, the MPLA method, which is limited to detection of deleted *FANCA* exons, is insufficient to fully characterize almost half the deletions in *FANCA*. The two largest deletions eliminated the largest number of surrounding genes in addition to the entire *FANCA* gene: the 545kb in *FAM9* eliminated 16 additional genes, four centromeric and twelve telomeric; the 478kb deletion in *FAM1* eliminated 18 additional genes, ten centromeric and eight telomeric (Figure 1, Supp. Table S2). The large hemizygous deletion (541 kb) in the *FANCB* family removed the entire *FANCB* as well as the neighboring *GLRA2* gene (Supp. Figure S1C). Identification of a larger number of such extended deletions would enable a reliable evaluation of whether the haplo-insufficiency (or complete loss) caused by the elimination of a subset of neighboring genes affects phenotypic heterogeneity or influences the clinical outcome of FA patients. As observed for a *FANCC* deletion (Chandrasekharappa, et al., 2013), the deletions removing the regulatory regions of *FANCA* may effect expression of the deletion-carrying allele, which can now be evaluated using a series of precise deletions identified in this study.

Three Quarters of the *FANCA* Deletions Appear to have Originated by NAHR

The identification of the exact nucleotide breakpoints provides insight into the mechanisms driving the deletion events in *FA* genes. Potential mechanisms leading to structural variants have been revealed, such as in the recent analysis of >2000 breakpoint junctions in the human genome (Kidd, et al., 2010) and somatic structural variations in human cancer genome from 140 patients (Yang, et al., 2013). We observed that 75% of the *FANCA* deletions are *Alu-Alu* mediated NAHR, while NHEJ (5%), alt-EJ (15%) and FoSTeS/MMBIR (5%) account for the rest (Table 4). *Alu-Alu* mediated NAHR is one of the most prevalent mechanisms driving recurrent intra-chromosomal recombination events in genomic disorders caused by deletions (Gu, et al., 2008; Liu, et al., 2011), and it seems to be the predominant mode for generating *FANCA* non-recurrent deletions as well. *Alu-Alu* mediated NAHR has been suggested to be the cause for majority of deletions in *VHL* (Franke, et al., 2009) and in *BRCA1* (Mazoyer, 2005). A majority of the non-recurrent deletions in the *FOXL2* gene region leading to the blepharophimosis syndrome (BPES), however, lacked extended homology and were found to involve mechanisms other than NAHR (Verdin, et al., 2013). About 20% of the *FANCA* deletions share no homology or very short homology (2–4 bp), and the mechanism driving these deletions may be explained by NHEJ (or alt-EJ), an imprecise DNA repair mechanism for double stranded breaks which does not require homology and tolerates addition of nucleotides at the joining sites (Lieber, 2008; Weterings and van Gent, 2004). Interestingly, one *FANCC* and three *FANCA* deletions with insertions of >10 bp at the breakpoints appear to be caused by FoSTeS/MMBIR, a replication based mechanism that involves stalling at replication forks and switching to a different template, and thus may involve more than two regions. In fact, two of the three *FANCA* deletions appear to involve three regions, reminiscent of a recent description of an *Alu*-mediated deletion involving *SOX10* regulatory elements associated with Wardenburg syndrome type 4 (Bondurand, et al., 2012). The precise mapping of the breakpoints as described here for gene regions with multiple deletions, will enhance our understanding of the origin of pathogenic variants.

Hotspots for Deletion Breakpoints in *AluY* SINE Elements at *FANCA* Introns 5, 17 And 21

The identification of the precise nucleotide breakpoint by sequencing across the breakpoint junctions confirmed that the majority of breaks in *FANCA* occur in *Alu* elements (122/136). This is not surprising given the high density of small interspersed nuclear elements (SINE) within the *FANCA* locus. Genome-wide *Alu* SINE elements account for 11% of the total human genome sequence; however, at the *FANCA* locus, SINE elements comprise nearly 40% of the total genomic sequence. The genome-wide distribution of various *Alu* subfamilies reveals *AluS* followed by the oldest *Alu* element, *AluJ*, are the most abundant, accounting for 6.4% and 2.5% of the total genome sequence, respectively. The youngest of the *Alu* subfamilies, *AluY* (Price, et al., 2004), is the least abundant subfamily at 1.5%; however, the distribution throughout the genome appears to be non-random (Grover, et al., 2003). *AluSx* and *AluY* are equally represented as the highest percentage of SINE sequence at the *FANCA* locus and for 150kb of the extended region encompassing the *FANCA* gene (Figure 3). Thus the equal distribution of *AluSx* and *AluY* is not limited solely to the *FANCA* gene in this region. Despite the fact that the *AluSx* and *AluY* elements are of equal

abundance across the *FANCA* region, the breakpoints preferentially occur in *AluY* elements. Indeed, *AluY* elements have 40% more breakpoints than *AluSx* elements, highlighting that *AluY* elements are preferred for *Alu*-mediated NAHR in *FANCA* (Figure 3). The increased homology among the *AluY* elements may favor them as predominant sites for intrachromosomal deletions. A study analyzing the deletion breakpoints associated with Von Hippel-Lindau (VHL) disease, also reported that an *AluY* element was involved in seven out of 33 deletions of the *VHL* gene region, and thus highly recombinogenic (Franke, et al., 2009).

Despite the high number of available *Alu* elements in this region, some elements are targeted in multiple unique deletion events. *Alu* elements with multiple breakpoints may represent potential hotspots for DNA breakage events in *FANCA*, particularly those containing breakpoints from four or more unique deletions (Figure 4, Supp. Table S6). We also identified clusters of *Alu* elements with multiple breakpoints at introns 5, 17, and 28 of *FANCA*; the highest density of breakpoints occurred at intron 17 with nine unique breakpoints within a 1Kb region. It is not clear why certain *Alu* elements are targeted multiple times or why there is a high density of breakpoints in certain locations within the *FANCA* gene. It does not appear to be solely dependent on the density of *Alu* elements, nor is there any discernible correlation with DNase hypersensitivity sites, which might indicate accessible DNA. It is possible that a higher order of chromatin structure and overall genomic architecture may influence the availability and proximity of elements for recombination events.

Our analysis of conserved deletions (CD) identified six deletions in *FANCA* and one deletion in *FANCC* that are identical in two or more seemingly unrelated families of full or partial Caucasian/European descent. The *FANCC* mutation discovered earlier by RNA analysis, and denoted as c.1–250del because it lacked the first 250bp from cDNA (Strathdee, et al., 1992), is in fact caused by this genomic deletion, encompassing exon 3. However, one conserved deletion (CD6) was found on two very different haplotypes from families of different ancestry, supporting its occurrence at two different times. Phylogenetic analysis of the deleted haplotypes with the HapMap CEU Phase 2 haplotypes reveals that CD2, CD4, CD5, and CD6.2 are relatively closer to each other. With the exception of CD6.1, the deleted alleles appear to be of very recent origin (Supp. Figure S3).

Although the majority of the *FANCA* deletions were unique and private, the high resolution CGH data revealed that many of the deletions might share a common breakpoint at one or both ends. Six deletions appear to have near identical breakpoint junctions shared in two or more families. Conservation of the breakpoint events may indicate hotspots for chromosomal breakage within or around the *FANCA* gene. Our haplotype analysis of the families with conserved deletions indicate that except for CD6 that arose independently in two families, the rest appear to be acquired through shared inheritance.

Array CGH is an integral component of a comprehensive strategy for identifying disease-causing variants in FA genes (Chandrasekharappa, et al., 2013). Our analysis here reveals the extent and the broad spectrum of deletions in multiple FA genes that contribute to the onset of FA. Efforts can now be made to discover the distinct pathogenic molecular events

caused by these variants, and to correlate these with associated phenotypic changes. The identification of precise breakpoints allows for quick screening of deletions in family members by PCR-based methods and provides insight into the mechanisms driving deletion mutations.

Supplementary Material

Refer to Web version on PubMed Central for supplementary material.

Acknowledgments

We acknowledge the support from the Intramural Program of the National Human Genome Research Institute, NIH, Bethesda, MD. EKF acknowledges an NIH FARE award. We thank Marypat Jones and Ursula Harper of the Genomics Core, NHGRI for performing SNP genotyping. ADA, AS and IFAR were supported in part by grant # UL1 TR000043 from the National Center for Advancing Translational Sciences (NCATS), National Institutes of Health (NIH) Clinical and Translational Science Award (CTSA) program. AS was funded by the Anderson Cancer Center at the Rockefeller University, Burroughs Wellcome Fund Career Award for Medical Scientists. AS is a Rita Allen Foundation, Irma T. Hirschl and Alexandrine and Alexander Sinsheimer Foundation scholar, and is a recipient of a Doris Duke Clinical Scientist Development Award. SCC was supported by a grant from the Fanconi Anemia Research Fund. Finally, we are most grateful to the individuals and families who participated in this study, and for the help of their physicians in enrolling them in the IFAR.

Grant support: Grant # UL1 TR000043 from NCATS, NIH CTSA program, and NHGRI Intramural Research Program, NIH.

References

- Ameziane N, Errami A, Leveille F, Fontaine C, de Vries Y, van Spaendonk RM, de Winter JP, Pals G, Joenje H. Genetic subtyping of Fanconi anemia by comprehensive mutation screening. *Hum Mutat.* 2008; 29:159–66. [PubMed: 17924555]
- Amouri A, Talmoudi F, Messaoud O, d'Enghien CD, Rekaya MB, Allegui I, Azaiez H, Kefi R, Abdelhak A, Meseddi SH, et al. High frequency of exon 15 deletion in the FANCA gene in Tunisian patients affected with Fanconi anemia disease: implication for diagnosis. *Mol Genet Genomic Med.* 2014; 2:160–5. [PubMed: 24689079]
- Auerbach AD. Fanconi anemia and its diagnosis. *Mutation research.* 2009; 668:4–10. [PubMed: 19622403]
- Auerbach AD, Greenbaum J, Pujara K, Batish SD, Bitencourt MA, Kokemohr I, Schneider H, Lobitz S, Pasquini R, Giampietro PF, et al. Spectrum of sequence variation in the FANCG gene: an International Fanconi Anemia Registry (IFAR) study. *Hum Mutat.* 2003; 21:158–68. [PubMed: 12552564]
- Barrett JC, Fry B, Maller J, Daly MJ. Haploview: analysis and visualization of LD and haplotype maps. *Bioinformatics.* 2005; 21:263–5. [PubMed: 15297300]
- Bogliolo M, Schuster B, Stoepker C, Derkunt B, Su Y, Raams A, Trujillo JP, Minguillon J, Ramirez MJ, Pujol R, et al. Mutations in ERCC4, encoding the DNA-repair endonuclease XPF, cause Fanconi anemia. *Am J Hum Genet.* 2013; 92:800–6. [PubMed: 23623386]
- Bondurand N, Fouquet V, Baral V, Lecerf L, Loundon N, Goossens M, Duriez B, Labrune P, Pingault V. Alu-mediated deletion of SOX10 regulatory elements in Waardenburg syndrome type 4. *European journal of human genetics : EJHG.* 2012; 20:990–4. [PubMed: 22378281]
- Callen E, Casado JA, Tischkowitz MD, Bueren JA, Creus A, Marcos R, Dasi A, Estella JM, Munoz A, Ortega JJ, et al. A common founder mutation in FANCA underlies the world's highest prevalence of Fanconi anemia in Gypsy families from Spain. *Blood.* 2005; 105:1946–9. [PubMed: 15522956]
- Castella M, Pujol R, Callen E, Trujillo JP, Casado JA, Gille H, Lach FP, Auerbach AD, Schindler D, Benitez J, et al. Origin, functional role, and clinical impact of Fanconi anemia FANCA mutations. *Blood.* 2011; 117:3759–69. [PubMed: 21273304]

- Centra M, Memeo E, d'Apolito M, Savino M, Ianzano L, Notarangelo A, Liu J, Doggett NA, Zelante L, Savoia A. Fine exon-intron structure of the Fanconi anemia group A (FAA) gene and characterization of two genomic deletions. *Genomics*. 1998; 51:463–7. [PubMed: 9721219]
- Chandrasekharappa SC, Lach FP, Kimble DC, Kamat A, Teer JK, Donovan FX, Flynn E, Sen SK, Thongthip S, Sanborn E, et al. Massively parallel sequencing, aCGH, and RNA-Seq technologies provide a comprehensive molecular diagnosis of Fanconi anemia. *Blood*. 2013; 121:e138–48. [PubMed: 23613520]
- Couch FJ, Nathanson KL, Offit K. Two decades after BRCA: setting paradigms in personalized cancer care and prevention. *Science*. 2014; 343:1466–70. [PubMed: 24675953]
- de Vries Y, Lwiwski N, Levitus M, Kuyt B, Israels SJ, Arwert F, Zwaan M, Greenberg CR, Alter BP, Joenje H, et al. A Dutch Fanconi Anemia FANCC Founder Mutation in Canadian Manitoba Mennonites. *Anemia*. 2012; 2012:865170. [PubMed: 22701786]
- Franke G, Bausch B, Hoffmann MM, Cybulla M, Wilhelm C, Kohlhase J, Scherer G, Neumann HP. Alu-Alu recombination underlies the vast majority of large VHL germline deletions: Molecular characterization and genotype-phenotype correlations in VHL patients. *Hum Mutat*. 2009; 30:776–86. [PubMed: 19280651]
- Grover D, Majumder PP, Rao CB, Brahmachari SK, Mukerji M. Nonrandom Distribution of Alu Elements in Genes of Various Functional Categories: Insight from Analysis of Human Chromosomes 21 and 22. *Molecular Biology and Evolution*. 2003; 20:1420–1424. [PubMed: 12832639]
- Gu W, Zhang F, Lupski JR. Mechanisms for human genomic rearrangements. *PathoGenetics*. 2008; 1:4. [PubMed: 19014668]
- Gunderson KL, Steemers FJ, Lee G, Mendoza LG, Chee MS. A genome-wide scalable SNP genotyping assay using microarray technology. *Nat Genet*. 2005; 37:549–54. [PubMed: 15838508]
- Kidd JM, Graves T, Newman TL, Fulton R, Hayden HS, Malig M, Kallicki J, Kaul R, Wilson RK, Eichler EE. A human genome structural variation sequencing resource reveals insights into mutational mechanisms. *Cell*. 2010; 143:837–47. [PubMed: 21111241]
- Kottemann MC, Smogorzewska A. Fanconi anaemia and the repair of Watson and Crick DNA crosslinks. *Nature*. 2013; 493:356–63. [PubMed: 23325218]
- Lee JA, Carvalho CM, Lupski JR. A DNA replication mechanism for generating nonrecurrent rearrangements associated with genomic disorders. *Cell*. 2007; 131:1235–47. [PubMed: 18160035]
- Levrán O, Doggett NA, Auerbach AD. Identification of Alu-mediated deletions in the Fanconi anemia gene FAA. *Hum Mutat*. 1998; 12:145–52. [PubMed: 9711872]
- Lieber MR. The Mechanism of Human Nonhomologous DNA End Joining. *Journal of Biological Chemistry*. 2008; 283:1–5. [PubMed: 17999957]
- Liu P, Lacaria M, Zhang F, Withers M, Hastings PJ, Lupski JR. Frequency of nonallelic homologous recombination is correlated with length of homology: evidence that ectopic synapsis precedes ectopic crossing-over. *Am J Hum Genet*. 2011; 89:580–8. [PubMed: 21981782]
- Mazoyer S. Genomic rearrangements in the BRCA1 and BRCA2 genes. *Hum Mutat*. 2005; 25:415–22. [PubMed: 15832305]
- Moghrabi NN, Johnson MA, Yoshitomi MJ, Zhu X, Al-Dhalimy MJ, Olson SB, Grompe M, Richards CS. Validation of Fanconi anemia complementation Group A assignment using molecular analysis. *Genetics in medicine : official journal of the American College of Medical Genetics*. 2009; 11:183–92. [PubMed: 19367192]
- Morgan NV, Essop F, Demuth I, de Ravel T, Jansen S, Tischkowitz M, Lewis CM, Wainwright L, Poole J, Joenje H, et al. A common Fanconi anemia mutation in black populations of sub-Saharan Africa. *Blood*. 2005; 105:3542–4. [PubMed: 15657175]
- Morgan NV, Tipping AJ, Joenje H, Mathew CG. High frequency of large intragenic deletions in the Fanconi anemia group A gene. *Am J Hum Genet*. 1999; 65:1330–41. [PubMed: 10521298]
- Neveling K, Endt D, Hoehn H, Schindler D. Genotype-phenotype correlations in Fanconi anemia. *Mutation research*. 2009; 668:73–91. [PubMed: 19464302]
- Price AL, Eskin E, Pevzner PA. Whole-genome analysis of Alu repeat elements reveals complex evolutionary history. *Genome Res*. 2004; 14:2245–52. [PubMed: 15520288]

- Stephens M, Donnelly P. A comparison of bayesian methods for haplotype reconstruction from population genotype data. *Am J Hum Genet.* 2003; 73:1162–9. [PubMed: 14574645]
- Stephens M, Smith NJ, Donnelly P. A new statistical method for haplotype reconstruction from population data. *Am J Hum Genet.* 2001; 68:978–89. [PubMed: 11254454]
- Strathdee CA, Gavish H, Shannon WR, Buchwald M. Cloning of cDNAs for Fanconi's anaemia by functional complementation. *Nature.* 1992; 358:434. [PubMed: 1641028]
- Tipping AJ, Pearson T, Morgan NV, Gibson RA, Kuyt LP, Havenga C, Gluckman E, Joenje H, de Ravel T, Jansen S, et al. Molecular and genealogical evidence for a founder effect in Fanconi anemia families of the Afrikaner population of South Africa. *Proc Natl Acad Sci U S A.* 2001; 98:5734–9. [PubMed: 11344308]
- Verdin H, D'Haene B, Beysen D, Novikova Y, Menten B, Sante T, Lapunzina P, Nevado J, Carvalho CM, Lupski JR, et al. Microhomology-mediated mechanisms underlie non-recurrent disease-causing microdeletions of the FOXL2 gene or its regulatory domain. *PLoS Genet.* 2013; 9:e1003358. [PubMed: 23516377]
- Weterings E, van Gent DC. The mechanism of non-homologous end-joining: a synopsis of synapsis. *DNA Repair.* 2004; 3:1425–1435. [PubMed: 15380098]
- Whitney MA, Saito H, Jakobs PM, Gibson RA, Moses RE, Grompe M. A common mutation in the FACC gene causes Fanconi anaemia in Ashkenazi Jews. *Nat Genet.* 1993; 4:202–5. [PubMed: 8348157]
- Yang L, Luquette LJ, Gehlenborg N, Xi R, Haseley PS, Hsieh CH, Zhang C, Ren X, Protopopov A, Chin L, et al. Diverse mechanisms of somatic structural variations in human cancer genomes. *Cell.* 2013; 153:919–29. [PubMed: 23663786]

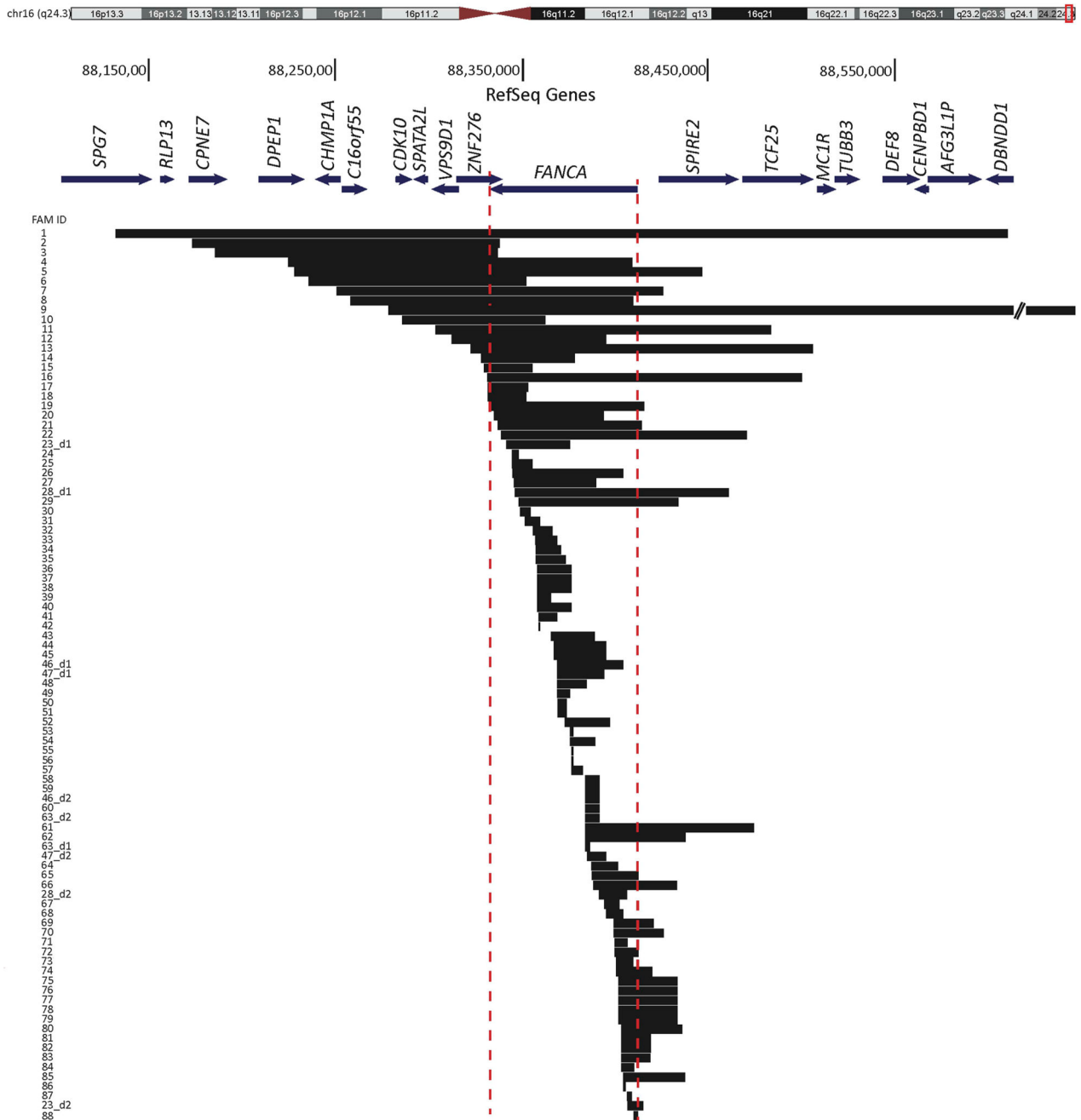


Figure 1. Extent of *FANCA* deletions in 88 FA families. BLAT alignment of deletion mutations involving *FANCA* and other surrounding genes identified in 88 FA families on UCSC genome browser (<http://genome.ucsc.edu>) (NCBI36/hg18). Chromosome 16 ideogram is shown at the top with the region of interest at q24.3 boxed in red. *FANCA* and neighboring genes are drawn to scale, and their transcription orientation is indicated by an arrow. Each horizontal block represents one distinct deletion and the family ID is indicated to the left. Families with two deletions are distinguished by “_d1” (for deletion 1) and “_d2” (for

deletion 2). Dotted vertical lines define the boundaries of *FANCA*. Twenty deletions originate centromeric and 32 terminate telomeric to *FANCA*, resulting in 47% of the deletions affecting genomic regions beyond the *FANCA* limits. Details of these deletions are in Table 2, Table 3, and Supp. Table S2.

Author Manuscript

Author Manuscript

Author Manuscript

Author Manuscript

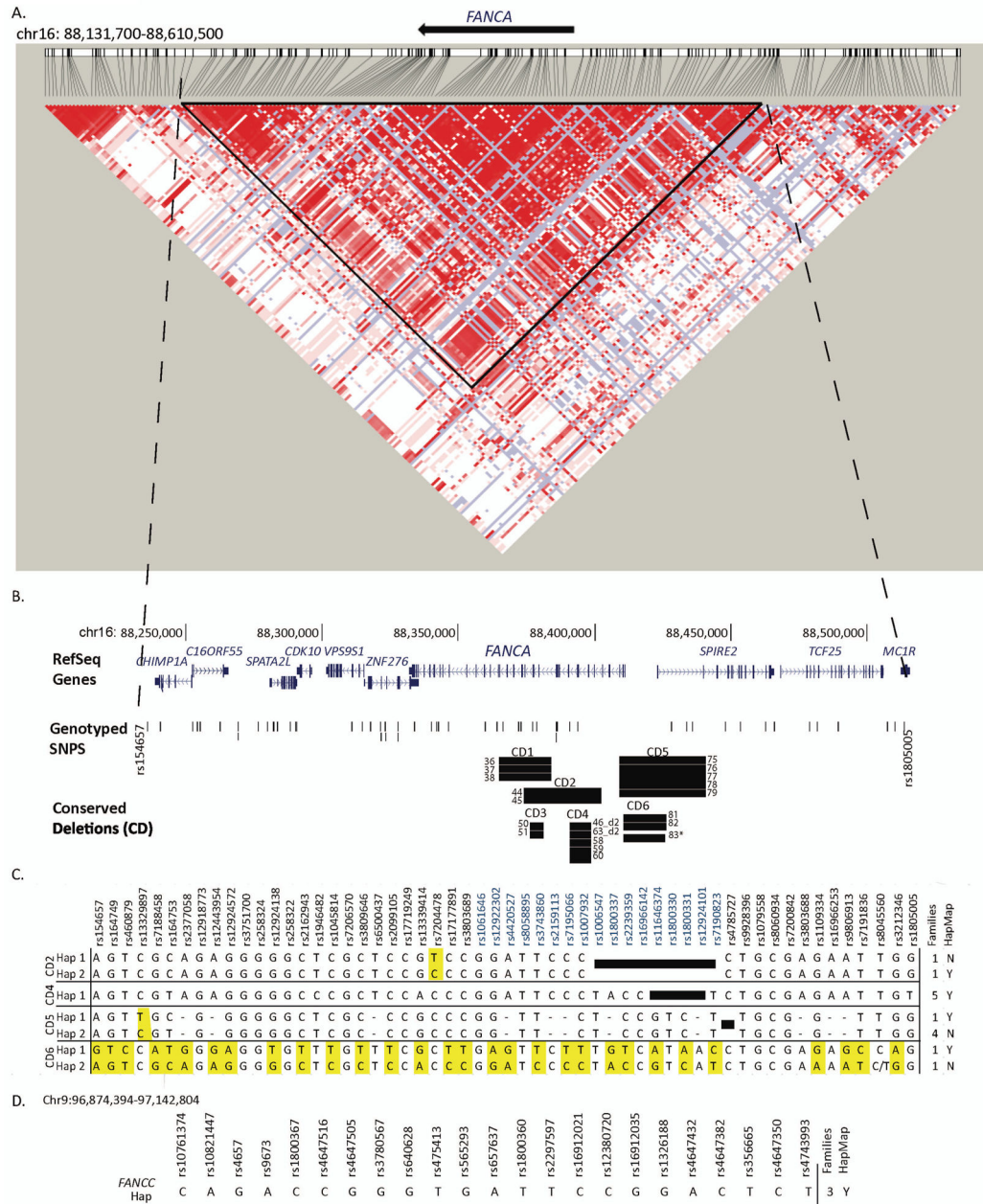


Figure 2.

Conserved deletions in *FANCA* and *FANCC*. **A.** HaploView generated LD plot of human chr16:88,130,00–88,610,500 (*FANCA* region). SNP data downloaded from HapMap Version 3 Release 2, CEU and TSI panel (<http://broadinstitute.org/haploview>) (Barrett, et al., 2005) Triangle indicates the one large LD block used for haplotype analysis. **B.** Location of RefSeq genes, genotyped SNPs and conserved deletions (CD) identified in *FANCA* families on UCSC genome browser NCBI36/hg18. RefSeq genes are drawn to scale, and vertical lines are exons and the arrows indicate the direction of transcription. Black bar represents

the deletion from one family and the Family IDs sharing the deletion are indicated. * indicates that the deletion in FAM83 is similar but not identical to the other members of CD6. **C.** Haplotypes on the specific allele carrying the conserved deletions. Haplotypes for four of the six conserved deletions are displayed. The SNP names are indicated by rs number, and those within the *FANCA* are in blue. Black boxes indicate SNPs that fall within the respective deleted regions. Number of families carrying the specific background haplotype and its presence (Y) or absence (N) in the HapMap Phase 2 phased haplotypes is indicated on the right. Differences between haplotypes for a given conserved deletion are highlighted in yellow. Dashed line indicates no SNP data. **D.** Haplotype of the *FANCC* allele carrying the conserved deletion in three FA families tested.

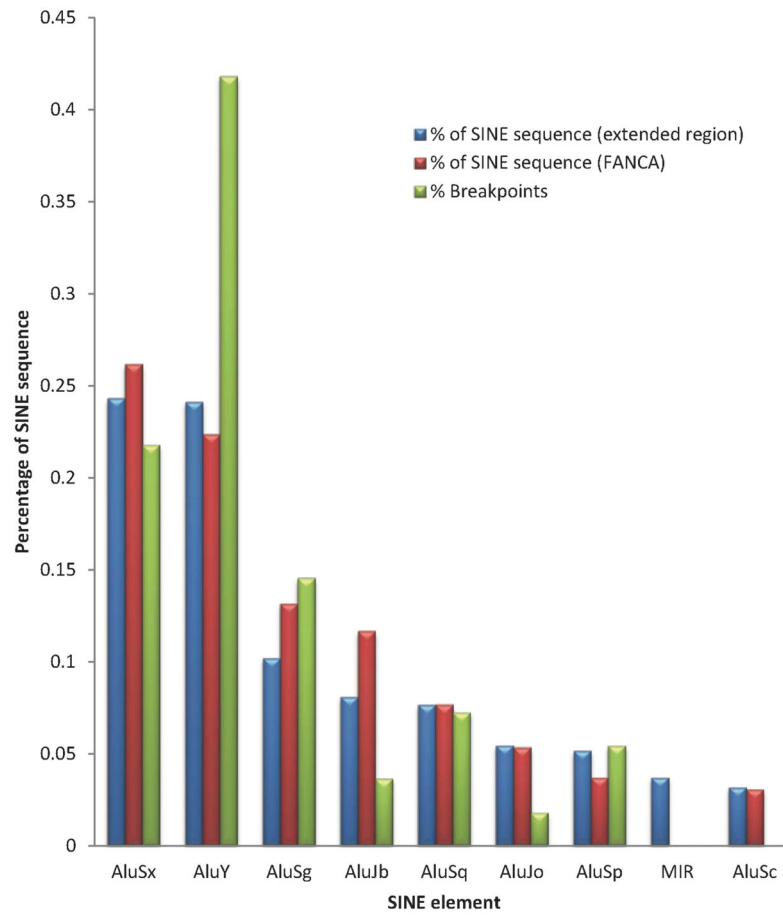


Figure 3.

FANCA Breakpoints preferentially occur in *AluY* elements. The distribution of the sequences (percent) from specific SINE elements in relation to the total SINE sequence within the *FANCA* (chr16.hg18:g.88331460_88410446) and the extended genomic region (chr16.hg18:g.88171112_88549994) are represented by blue and red bars respectively. The distribution (percent) of breakpoints in specific SINE elements is shown by green bars.

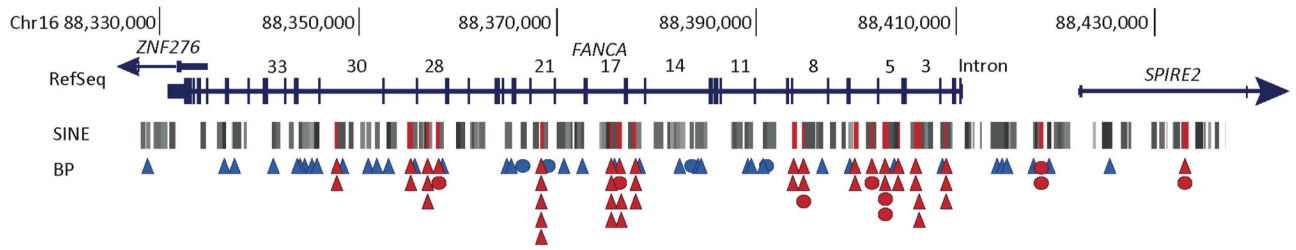


Figure 4.

Alu elements with multiple breakpoints indicate hotspots for *FANCA* deletions. Breakpoints in and around *FANCA* identified by cloning and sequencing are displayed along with the distribution of *Alu* elements. Exons are vertical lines, and the introns are numbered for *FANCA*. The SINE track from the UCSC Genome Browser NCBI36/hg18 (Repeat Masker track) is displayed. *Alu* elements with multiple breakpoints are highlighted in red. A triangle shows each unique breakpoint in a given *Alu* element. Circles show the *Alu* elements with breakpoints from conserved deletions, a circle for each conserved deletion (CD1–CD5) except two for CD6. Blue and red triangles and circles indicate a single and multiple breakpoints within a given *Alu* element respectively. Details of the *Alu* elements with multiple hits are in Supp. Table S6.

Table 1

Summary of Deletion Screen of 202 FA Families

A. All 202 FA Families

Gene	Deletion Type	Families with Deletion
<i>FANCA</i>	heterozygous	78
	homozygous	5
	compound heterozygous	5
<i>FANCB</i>	hemizygous	1
<i>FANCC</i>	heterozygous	7
<i>FANCD2</i>	heterozygous	2

B. The Subset of 105 FA Families With No Prior Knowledge of Affected Gene or Mutations

Gene	Deletion Type	Families with Deletion
<i>FANCA</i>	heterozygous	32
	homozygous	1
	compound heterozygous	1
<i>FANCD2</i>	heterozygous	2

Author Manuscript

Author Manuscript

Author Manuscript

Author Manuscript

Table 2

Deletion Intervals in FA Genes Determined by aCGH

Family ID	Number of Deletions	Gene	Chr	Deletion Start	Deletion End	BPs	Deleted Exons
1	1	FANCA	16	88,131,700	88,610,500	478,801	1-43
3	1	FANCA	16	88,184,848	88,336,349	151,502	38-43
5	1	FANCA	16	88,227,499	88,446,249	218,751	1-43
6	1	FANCA	16	88,235,249	88,351,749	116,501	31-43
9 [§]	1	FANCA	16	88,281,756	88,827,254	545,499	1-43
12	2 HO	FANCA	16	88,311,999	88,394,999	83,001	9-43
16	1	FANCA	16	88,330,849	88,500,000	169,152	1-43
20	1	FANCA	16	88,334,499	88,393,249	58,751	10-38
22	1	FANCA	16	88,338,249	88,470,249	132,001	1-36
41	1	FANCA	16	88,358,548	88,368,349	9,802	22-28
42	1	FANCA	16	88,358,574	88,359,274	701	28
43	1	FANCA	16	88,364,999	88,388,499	23,501	12-23
61	1	FANCA	16	88,383,499	88,474,299	90,801	1-14
62	1	FANCA	16	88,383,499	88,437,499	54,001	1-14
63_d1	2 HE	FANCA	16	88,383,649	88,386,149	2,501	13-14
64	1	FANCA	16	88,386,749	88,401,249	14,501	7-11
65	1	FANCA	16	88,387,000	88,412,000	25,001	1-11
66	1	FANCA	16	88,387,749	88,432,749	45,001	1-11
69	1	FANCA	16	88,398,749	88,420,249	21,501	1-7
70	1	FANCA	16	88,398,749	88,425,749	27,001	1-7
72	1	FANCA	16	88,399,249	88,412,249	13,001	1-7
84	1	FANCA	16	88,403,105	88,410,000	6,896	2-5
85	1	FANCA	16	88,403,999	88,437,249	33,251	1-5
86	1	FANCA	16	88,404,000	88,405,000	1,001	4-5
88	1	FANCA	16	88,409,549	88,411,749	2,201	1-2
89	1	FANCC	9	96,935,249	96,937,749	2,501	8
96 [§]	1	FANCB	X	14,331,665	14,872,323	540,659	1-10
97	1	FANCD2	3	10,048,249	10,066,749	18,501	2-17

Family ID	Number of Deletions	Gene	Chr	Deletion Start	Deletion End	BP's	Deleted Exons
98	1	FANCD2	3	10,066,800	10,071,613	4,813	18

This table excludes deletion intervals that were defined by cloning and sequencing, which are presented in Table 3.

§ denotes breakpoints for deletion determined by SNP array.

Families with two deleted alleles are indicated with 2 in "Number of Deletions" column.

HO = Homozygous

HE = Compound Heterozygous (and distinguished by "_d1" for deletion 1)

The deletion coordinates are according to the NCBI36/hg18 build.

Table 3
Exact Breakpoint Coordinates and Characteristics of Deletions Determined by Cloning and Sequencing in FA Families

FAM ID	No.	FA Gene	Start	End	size (bps)	Cen Rep	Cen Rep Start	Cen Rep End	+/-	Tel Rep	Tel Rep Start	Tel Rep End	+/-	Overlap or Insertion bps*	Potential Mechanism	Alu - Alu	Exons
2	1	A	88,172,538	88,337,600	165,063	AluSx	88,172,387	88,172,690	+	AluSp	88,337,451	88,337,757	+	11	NAHR	Y	37-43
4	1	A	88,224,066	88,408,991	184,926	NR				AluSx	88,408,947	88,409,245	-	3	alt-EJ	N	3-43
7	1	A	88,250,100	88,425,360	175,261	AluY	88,250,056	88,250,345	-	AluY	88,425,297	88,425,605	-	27	NAHR	Y	1-43
8	1	A	88,257,445	88,409,236	151,792	AluSp	88,257,167	88,257,453	-	AluSx	88,408,947	88,409,245	-	26	NAHR	Y	3-43
10	1	A	88,285,490	88,362,122	76,633	NR				NR				2	alt-EJ	N	27-43
11	1	A	88,302,909	88,483,387	180,479	NR				NR				4	alt-EJ	N	1-43
13	1	A	88,322,270	88,505,839	183,570	AluSx	88,322,116	88,322,301	-	AluY	88,505,703	88,506,000	-	24	NAHR	Y	1-43
14	1	A	88,327,695	88,377,962	50,268	NR				AluSp	88,377,678	88,377,968	-	2	alt-EJ	N	16-43
15	1	A	88,329,020	88,355,305	26,286	AluSx	88,328,786	88,329,049	+	AluY	88,355,047	88,355,357	+	11	NAHR	Y	30-43
17	1	A	88,331,201	88,352,999	21,799	AluSg	88,331,149	88,331,450	+	AluY	88,352,948	88,353,258	+	4	NAHR	Y	30-43
18	1	A	88,331,357	88,351,875	20,519	AluSg	88,331,149	88,331,450	+	AluSx	88,351,789	88,352,065	-	2	alt-EJ	Y ^o	31-43
19	1	A	88,331,930	88,415,141	83,212	NR				AluSx	88,415,082	88,415,384	-	2	alt-EJ	N	1-43
21	1	A	88,336,484	88,414,112	77,629	AluY	88,336,437	88,336,568	+	AluSx	88,414,066	88,414,360	+	36	NAHR	Y	1-37
23_d1	2 HE	A	88,341,384	88,375,356	33,973	AluSg	88,341,341	88,341,647	+	AluY	88,375,302	88,375,614	+	21	NAHR	Y	18-33
24	2 HO	A	88,344,051	88,347,742	3,692	AluJ FLAM	88,343,990	88,344,068	+	AluSx	88,347,682	88,347,981	+	31	NAHR	Y	31
25	1	A	88,344,194	88,355,131	10,938	AluY	88,344,109	88,344,414	+	AluY	88,355,047	88,355,357	+	7	NAHR	Y	30-31
26	2 HO	A	88,344,637	88,404,186	59,550	AluSg	88,344,416	88,344,697	+	AluSx	88,403,786	88,403,949	+	17	NAHR	Y	6-31
27	1	A	88,345,159	88,389,286	44,128	AluJb	88,345,131	88,345,394	+	AluSx	88,389,257	88,389,566	+	10	NAHR	Y	12-31
28_d1	2 HE	A	88,345,766	88,460,603	114,838	AluY	88,345,678	88,345,977	-	AluY	88,460,509	88,460,817	-	45	NAHR	Y	1-31
29	1	A	88,347,917	88,433,278	85,362	AluSx	88,347,682	88,347,981	+	AluY	88,432,969	88,433,298	+	11	NAHR	Y	1-30
30	1	A	88,348,428	88,353,975	5,548	AluSg	88,348,275	88,348,577	-	NR				ins. 37bps	FoSTeS/MMBIR	N	30
31	1	A	88,351,156	88,359,359	8,204	AluSx	88,350,890	88,351,168	-	NR				ins. 29bps	FoSTeS/MMBIR	N	28-30
32	1	A	88,355,680	88,365,679	10,000	AluJb	88,355,542	88,355,833	-	FANCA exon23	88,365,587	88,365,723		2	alt-EJ	N	23-29
33	1	A	88,356,841	88,368,468	11,628	AluY	88,356,875	88,357,188	+	AluY	88,368,358	88,368,663	+	21	NAHR	Y	22-28
34	1	A	88,356,984	88,370,562	13,579	AluY	88,356,875	88,357,188	+	AluY	88,370,455	88,370,769	+	44	NAHR	Y	21-28
35	1	A	88,356,998	88,373,127	16,130	AluY	88,356,875	88,357,188	+	AluY ^{INS}	AluY ^{INS}	88,373,127	+	ins. 179bps	FoSTeS/MMBIR	Y	19-28

FAM ID	No.	FA Gene	Start	End	size (bps)	Cen Rep	Cen Rep Start	Cen Rep End	+/-	Tel Rep	Tel Rep Start	Tel Rep End	+/-	Overlap or Insertion bps*	Potential Mechanism	Alu - / Alu	Exons
36	1	A	88,357,692	88,376,135	18,444	AluSg	88,357,566	88,357,859	+	AluY	88,376,003	88,376,138	+	4	NAHR	Y	18-28
37	1	A	88,357,692	88,376,135	18,444	AluSg	88,357,566	88,357,859	+	AluY	88,376,003	88,376,138	+	4	NAHR	Y	18-28
38	1	A	88,357,692	88,376,135	18,444	AluSg	88,357,566	88,357,859	+	AluY	88,376,003	88,376,138	+	4	NAHR	Y	18-28
39	1	A	88,357,733	88,365,259	7,527	AluSg	88,357,566	88,357,859	+	AluJb	88,365,086	88,365,390	+	20	NAHR	Y	18-24
40	1	A	88,357,923	88,376,192	18,270	AluSq	88,357,872	88,358,166	+	AluY	88,376,003	88,376,138	+	12	NAHR	Y	18-28
44	1	A	88,366,653	88,394,866	28,214	AluSx	88,366,445	88,366,750	+	AluSx	88,394,658	88,394,971	+	10	NAHR	Y	9-22
45	1	A	88,366,653	88,394,866	28,214	AluSx	88,366,445	88,366,750	+	AluSx	88,394,658	88,394,971	+	10	NAHR	Y	9-22
46_d1	2 HE	A	88,368,466	88,404,057	35,592	AluY	88,368,358	88,368,663	+	AluY	88,403,951	88,404,249	+	28	NAHR	Y	6-21
47_d1	2 HE	A	88,368,481	88,393,743	25,263	AluY	88,368,358	88,368,663	+	AluY	88,393,654	88,393,920	+	14	NAHR	Y	9-21
48	1	A	88,368,519	88,384,182	15,664	AluY	88,368,358	88,368,663	+	AluSx	88,384,029	88,384,350	+	8	NAHR	Y	15-21
49	1	A	88,368,578	88,375,523	6,946	AluY	88,368,358	88,368,663	+	AluY	88,375,302	88,375,614	+	14	NAHR	Y	18-21
50	1	A	88,368,840	88,373,628	4,789	AluSx	88,368,721	88,369,009	+	NR	NR	NR	NR	2	alt-EJ	N	18-21
51	1	A	88,368,840	88,373,628	4,789	AluSx	88,368,721	88,369,009	+	NR	NR	NR	NR	2	alt-EJ	N	18-21
52	1	A	88,372,488	88,396,714	24,227	AluSg x	88,372,403	88,372,566	+	LINE	88,396,612	88,397,058	+	none	NHEJ	N	9-20
53	1	A	88,375,333	88,377,211	1,879	AluY	88,375,302	88,375,614	+	AluY	88,377,178	88,377,485	+	13	NAHR	Y	16-17
54	1	A	88,375,502	88,389,110	13,609	AluY	88,375,302	88,375,614	+	AluSx	88,388,912	88,389,192	+	22	NAHR	Y	12-17
55	1	A	88,376,050	88,377,224	1,175	AluY	88,375,627	88,375,930	+	AluY	88,377,178	88,377,485	+	22	NAHR	Y	16-17
56	1	A	88,376,126	88,377,300	1,175	AluY	88,376,139	88,376,434	+	AluY	88,377,178	88,377,485	+	14	NAHR	Y	16-17
57	1	A	88,376,281	88,382,229	5,949	AluY	88,376,139	88,376,434	+	AluSc	88,382,090	88,382,369	+	10	NAHR	Y	15-17
46_d2	2 HE	A	88,383,475	88,391,064	7,590	AluJo	88,383,349	88,383,647	-	AluY	88,390,786	88,391,090	+	ins. 2bps	NHEJ	Y ^o	11-14
63_d2	2 HE	A	88,383,475	88,391,064	7,590	AluJo	88,383,349	88,383,647	-	AluY	88,390,786	88,391,090	+	ins. 2bps	NHEJ	Y ^o	11-14
58	1	A	88,383,475	88,391,064	7,590	AluJo	88,383,349	88,383,647	-	AluY	88,390,786	88,391,090	+	ins. 2bps	NHEJ	Y ^o	11-14
59	1	A	88,383,475	88,391,064	7,590	AluJo	88,383,349	88,383,647	-	AluY	88,390,786	88,391,090	+	ins. 2bps	NHEJ	Y ^o	11-14
60	1	A	88,383,475	88,391,064	7,590	AluJo	88,383,349	88,383,647	-	AluY	88,390,786	88,391,090	+	ins. 2bps	NHEJ	Y ^o	11-14
47_d2	2 HE	A	88,384,547	88,394,863	10,317	AluSg	88,384,358	88,384,675	+	AluSx	88,394,658	88,394,971	+	23	NAHR	Y	9-14
28_d2	2 HE	A	88,390,697	88,406,009	15,313	AluSg	88,390,650	88,390,785	+	AluY	88,405,963	88,406,268	+	8	NAHR	Y	4-10
67	1	A	88,393,778	88,401,667	7,890	AluY	88,393,654	88,393,920	+	AluY	88,401,513	88,401,817	+	12	NAHR	Y	7-8
68	1	A	88,394,840	88,404,129	9,290	AluSx	88,394,658	88,394,971	+	AluY	88,403,951	88,404,249	+	20	NAHR	Y	6-8
71	1	A	88,399,194	88,406,309	7,116	FANCA exon7	88,399,189	88,399,301	-	AluSp	88,406,274	88,406,579	+	1	NHEJ	N	4-7
73	1	A	88,399,898	88,409,021	9,124	AluSq	88,399,826	88,400,121	-	AluSx	88,408,947	88,409,245	-	5	NAHR	Y	3-6

FAM ID	No.	FA Gene	Start	End	size (bps)	Cen Rep	Cen Rep Start	Cen Rep End	+/-	Tel Rep	Tel Rep Start	Tel Rep End	+/-	Overlap or Insertion bps*	Potential Mechanism	Alu - Alu	Exons
74	2 HO	A	88,400,101	88,419,559	19,459	AluSq	88,399,826	88,400,121	-	AluY	88,419,273	88,419,580	-	26	NAHR	Y	1-6
75	1	A	88,401,663	88,433,153	31,491	AluY	88,401,513	88,401,817	+	AluY	88,432,969	88,433,298	+	13	NAHR	Y	1-6
76	1	A	88,401,663	88,433,153	31,491	AluY	88,401,513	88,401,817	+	AluY	88,432,969	88,433,298	+	13	NAHR	Y	1-6
77	1	A	88,401,663	88,433,153	31,491	AluY	88,401,513	88,401,817	+	AluY	88,432,969	88,433,298	+	13	NAHR	Y	1-6
78	1	A	88,401,663	88,433,153	31,491	AluY	88,401,513	88,401,817	+	AluY	88,432,969	88,433,298	+	13	NAHR	Y	1-6
79	1	A	88,401,663	88,433,153	31,491	AluY	88,401,513	88,401,817	+	AluY	88,432,969	88,433,298	+	13	NAHR	Y	1-6
80	1	A	88,402,939	88,435,730	32,792	AluY	88,402,820	88,403,114	-	AluSp	88,435,611	88,435,932	-	13	NAHR	Y	1-5
81	2 HO	A	88,403,094	88,418,774	15,681	AluY	88,402,820	88,403,114	-	AluSg	88,418,482	88,418,795	-	27	NAHR	Y	1-5
82	1	A	88,403,094	88,418,774	15,681	AluY	88,402,820	88,403,114	-	AluSg	88,418,482	88,418,795	-	27	NAHR	Y	1-5
83	1	A	88,403,104	88,418,467	15,364	AluY	88,402,820	88,403,114	-	AluSc	88,418,349	88,418,478	-	46	NAHR	Y	1-5
87	1	A	88,406,084	88,408,690	2,607	AluY	88,405,963	88,406,268	+	AluSg	88,408,570	88,408,879	+	22	NAHR	Y	3
23_d2	2 HE	A	88,406,326	88,414,712	8,387	AluSp	88,406,274	88,406,579	+	AluSq2	88,414,671	88,414,970	+	31	NAHR	Y	1-3
90	1	C	97,046,452	97,050,240	3,789	NR				AluY	97,046,501	97,046,811	+	ins. 18bps	FoSTeS/MMBIR	N	3
91	1	C	97,046,452	97,050,240	3,789	NR				AluY	97,046,501	97,046,811	+	ins. 18bps	FoSTeS/MMBIR	N	3
92	1	C	97,046,452	97,050,240	3,789	NR				AluY	97,046,501	97,046,811	+	ins. 18bps	FoSTeS/MMBIR	N	3
93	1	C	97,046,452	97,050,240	3,789	NR				AluY	97,046,501	97,046,811	+	ins. 18bps	FoSTeS/MMBIR	N	3
94	1	C	97,046,452	97,050,240	3,789	NR				AluY	97,046,501	97,046,811	+	ins. 18bps	FoSTeS/MMBIR	N	3
95	1	C	97,115,943	97,125,170	9,228	NR				MLT1J MaLR	97,125,086	97,125,394	+	ins. 1bp	NHEJ	N	1

Foot notes in Table 2 also apply here. Cen and Tel represent centromeric and telomeric ends of a deletion. The Start is the Cen breakpoint and contains any overlap sequence.

The End coordinate is the Tel breakpoint and contains none of the overlap sequence.

Strand (+/-) indicates the orientation of the repeat element. Y/O =yes in opposite orientation. Identical deletions are shaded in gray.

*The precise sequence of the Overlap or Insertion bps is provided in Table S4

The Criteria for "potential mechanism" are as described in Yang et al., (2013, Cell)

The deletion coordinates are according to the NCBI36/hg18 build.

Table 4

Breakdown of Likely Mechanisms Causing Deletions in FA Genes

Gene	Proposed Mechanism**	Non-Recurrent	Recurrent	Percentage	Observed Breakpoint Characteristics
FANCA *	FoStEs/MMBIR	3	0	5	insertions of 29, 34 and 178 bases
	NHEJ	2	1	5	homology of 0–2 bases or insertion of 1–2 bases
	alt-EJ	7	1	15	homology of 2, 3 or 4 bases
	NAHR	37	4	75	<i>Alu-Alu</i> repeats in the same orientation
FANCC	FoStEs/MMBIR	0	1	--	insertions of 18 bases
	NHEJ	1	0	--	insertion of one base

* The 68 FANCA deletions accounted for 55 distinct breakpoints

** Criteria for determining mechanism (as described in Yang et al., 2013, Cell)

NHEJ Deletion breakpoints have an insertion 1–10 bp or homology < 2 bp

FoStEs/MMBIR Deletion breakpoints have an insertion > 10 bp

alt-EJ Deletion breakpoints do not have an insertion and homology 2–100 bp

NAHR Deletion breakpoints do not have an insertion but have an homology > 100 bp